Supporting Information

Dimeric polybismuthide heteroanion of $[Rh@Bi_{10}(RhCO)_5]^{2-}$ built of Bi_{10}-bowl and $Rh@(Rh\text{-}CO)_5$ square pyramidal

Yipeng Zang,a,b Yueyue Wang,a,b Ruili Sanga and Li Xu*a

[a]State Key Laboratory of Structural Chemistry, Fujian Institute of Research on the Structure of Matter, Chinese Academy of Sciences, Fuzhou, Fujian, 350002.

[b]University of Chinese Academy of Sciences Beijing 100049 (China)

E-mail: xli@fjirsm.ac.cn.

Table of Contents

S1. Experimental Details

All manipulations were carried out under argon using the standard Schlenk-line and glovebox techniques. Ethylenediamine (Acros, 99%) was distilled over sodium metal and stored in a gastight Schlenk under argon in the glovebox. Toluene was dried with potassium-sodium alloy and then stored in the glovebox. Precursors with nominal composition K_5Bi_4 [1]was synthesized by fusion of stoichiometric ratios of the elements (K: +99%; Bi: 99.999 %, all from Strem) at ~1100℃ for few minutes. The elements were loaded into quartz tubes and were sealed in the argon atomesphere glovebox. 2,2,2-Crypt (2,2,2-Crypt=4,7,13,16,21,24-hexaoxa-1,10-diazabicyclo[8.8.8]hexacosane) (accela, 99%), $Rh_2(CO)_4Cl_2$ (Aladdin,97%) were used as received.

Single crystal X-ray crystallography. Single crystal X-ray diffraction data of [Rh2@Bi20(RhCO)10]4-(1) was recorded on a Bruker Apex CCD diffractometer (λ (MoKα) = 0.71073 Å) at 160 K equipped with a graphite monochromator. Data collection and reduction were performed using the Apex2 software package and the structure was solved by direct method using the SHELXS program of the SHELXTL package and refined by full-matrix least-squares on F2 with SHELXL-2014. Corrections for incident and diffracted beam absorption effects were applied using multi-scan correction. All subject atoms Bi, Rh were refined anisotropically except for the guest molecules. More detailed information on the 1 crystal structure can be obtained from Table 1, Tables 7 - 9, Figures S3 -S5 of the Supporting Information. CCDC 2216599 (1) contain the supplementary crystallographic data.

Synthesis of $[K(2,2,2\text{-Crypt})]_4[Rh@Bi_{10}(RhCO)_5]_2\cdot 3en$ ($[K(2,2,2\text{-Crypt})]_4\cdot[1]\cdot 3en$): The binary alloy with the nominal composition K_5Bi_4 (40 mg, 0.0388 mmol) and 2,2,2-Crypt (30 mg, 0.08 mmol) were dissolved in 2 mL ethylenediamine in a test tube and stirred for 0.5 hours at room temperature, yielding a dark green solution. Then $Rh_2(CO)_4Cl_2$ (5 mg, 0.013 mmol) was added to the solution, and the mixture solution immediately turned red-brown and was allowed to stir for approximately 4 h at room temperature. The resulting red-brown solution was filtered using a glass fiber pipette and the filtrate was layered with toluene (7 ml). Black block crystal of 1 (2 mg, 11.2% based on Rh) were obtained after about a month. Calcd. for $C_{88}H_{140}Bi_{20}K_4N_{14}O_{34}Rh_{12}$ (Mr= 7509.05): C 14.06%, H 1.86%, N 2.61; Found: C 15.16%, H 2.06%, N 2.30%.

Table S1. Crystallographic data of $[K(2,2,2\text{-Crypt})]_4[\mathbf{1}]\cdot 3en$.

Empirical formula	$C_{88}H_{140}Bi_{20}K_4N_{14}O_{34}Rh_{12}$
Formula weight	7509.05
Temperature	160(02) K
Wavelength	0.71073 Å
Crystal system	Triclinic
Space group	P-1
a/ Å	16.6076(15)
b/ Å	17.1151(16)
c / Å	29.840(3)
α/°	97.547(3)
β/°	101.929(3)
γ/°	100.646(3)
Volume	8028.0(13) $Å^3$
Z	2
$\rho_{calc}(mg/m^3)$	3.106
μ/ mm^{-1}	23.183
F (000)	6628.0
Crystal size(mm^3)	0.2000×0.100×0.100
2Θ range for data collection/°	4.514 to 47.858
Index ranges	-18 ≤ h ≤ 18, -19 ≤ k ≤ 19, -34 ≤ l ≤ 33
Reflections collected	98743
Independent reflections	24727 [R_{int}= 0.0986, R_{sigma}= 0.0783]
Completeness	99.0%
Data/restraints/parameters	24727/80/1549
Goodness-of-fit on F2	1.019
Final R indexes [I>=2σ (I)]	R1 = 0.0485, wR2 = 0.1006
Final R indexes [all data]	R1 = 0.0759, wR2 = 0.1132

S2. Energy Dispersive X-ray (EDX) Spectroscopy

The energy-dispersive X-ray spectroscopy (EDX, JEOLSEM, JSM-6700F) analyses of the single crystals of $[K(2,2,2\text{-Crypt})]_4[1]$, which indicated that that the elements K, Rh and Bi are present approximately in the expected ratio of 4:12:20(or2:6:10).

Table S2. EDX analysis of $[K(2,2,2\text{-Crypt})]_4$[**1**]·3*en*.

Element	Weight %	Atom %	Ratio
K	2.79	11.12	2
Rh	21.36	32.34	5.92
Bi	75.85	55.54	10.23

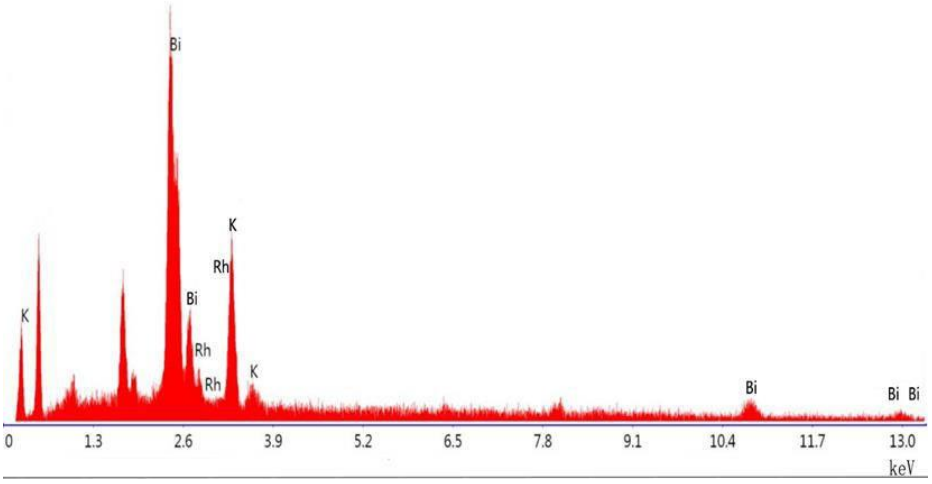

Figure S1. EDX spectrum of $[K(2,2,2\text{-Crypt})]_4$[**1**]·3*en*.

S3. IR spectra of 1

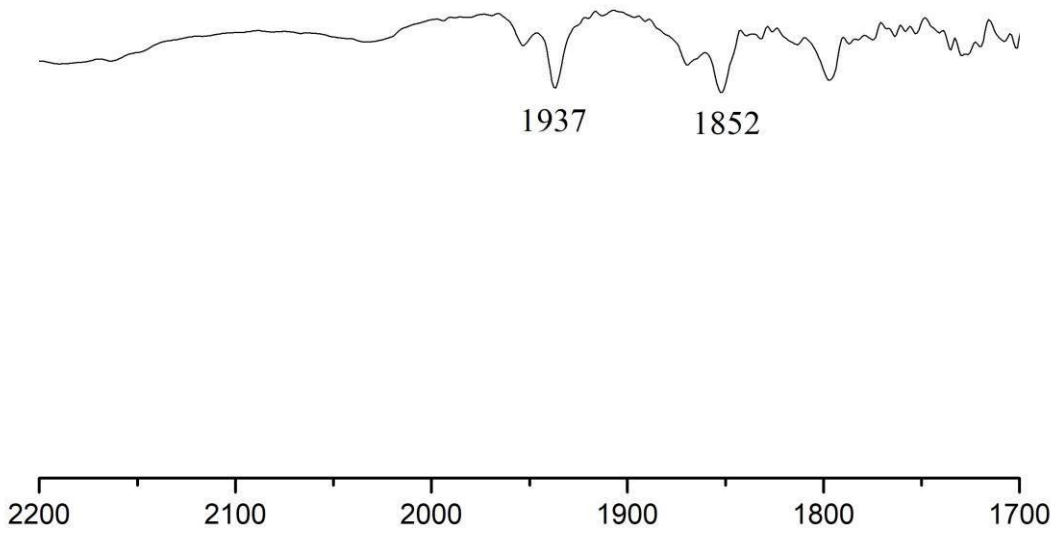

Figure S2. IR of **1** recorded as KBr pellets in Nujol mulls on a Magna 750 FT-IR spectrometer photometer.

S4. ICP of 1.

Table S3. The ICP result of **1** recorded on a Ultima2, HORIBA Jobin Yvon, Germany.

Element	Measured mg/L	Weight %	Cal.Weight %
K	5.24	3.87	2.81
Rh	31.59	23.33	22.16
Bi	98.60	72.81	75.03

S5. Crystal structures of 1 and 1a.

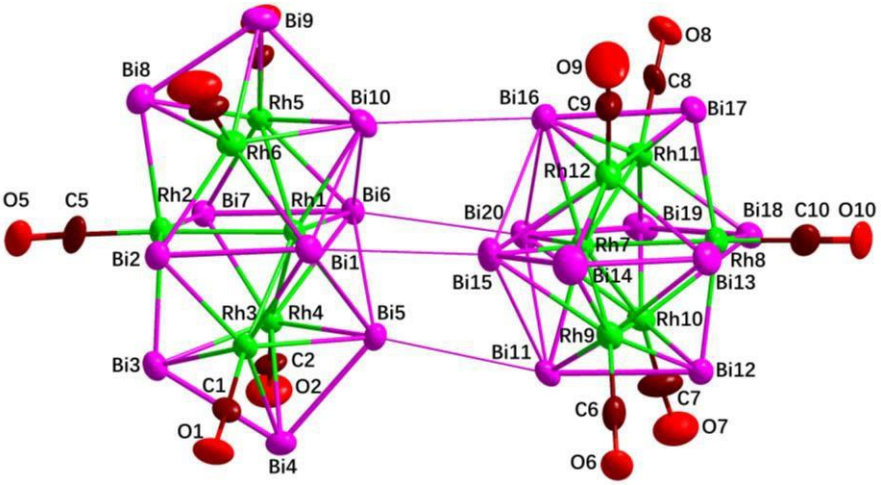

Figure S3. Structure of **1** with 50% thermal ellipsoids.

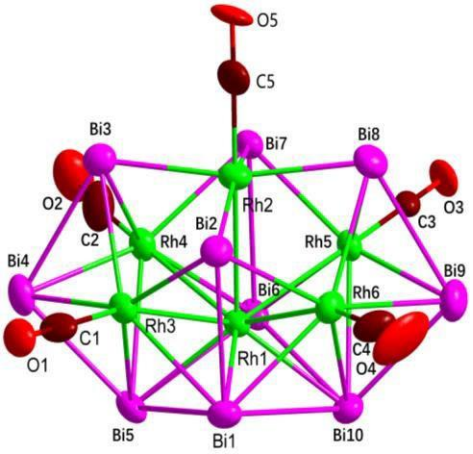

Figure S4. Structure of **1a** with 50% thermal ellipsoids.

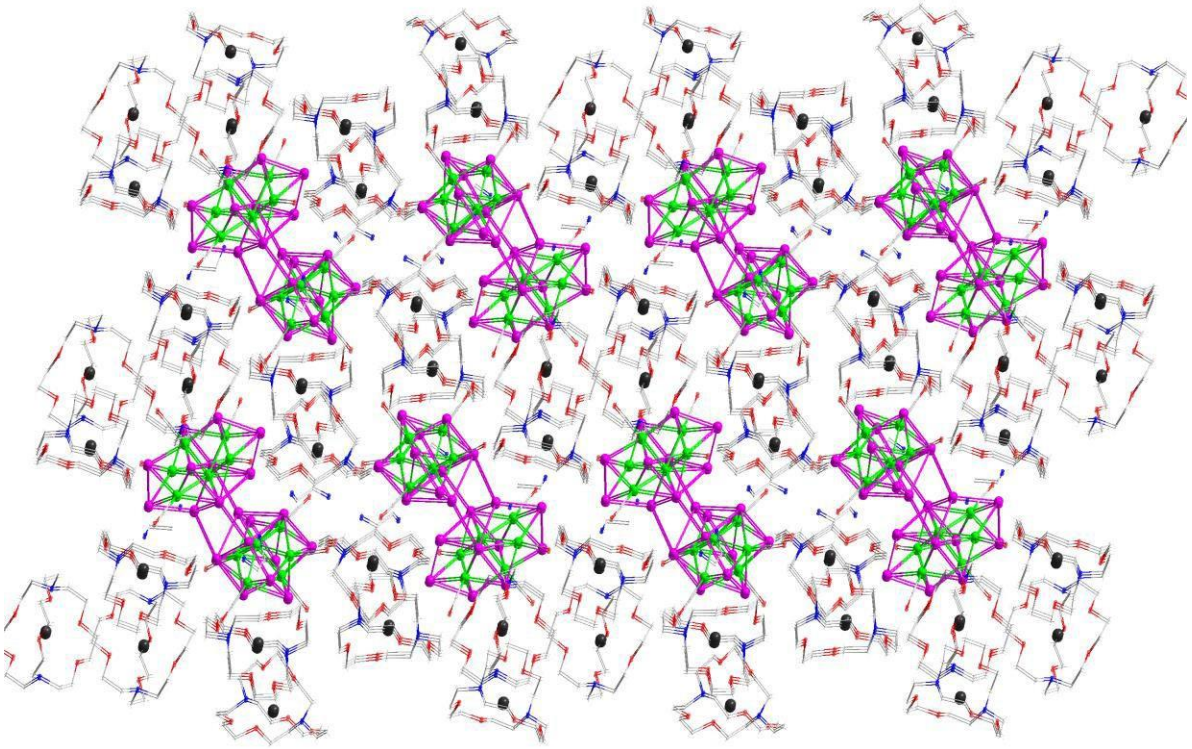

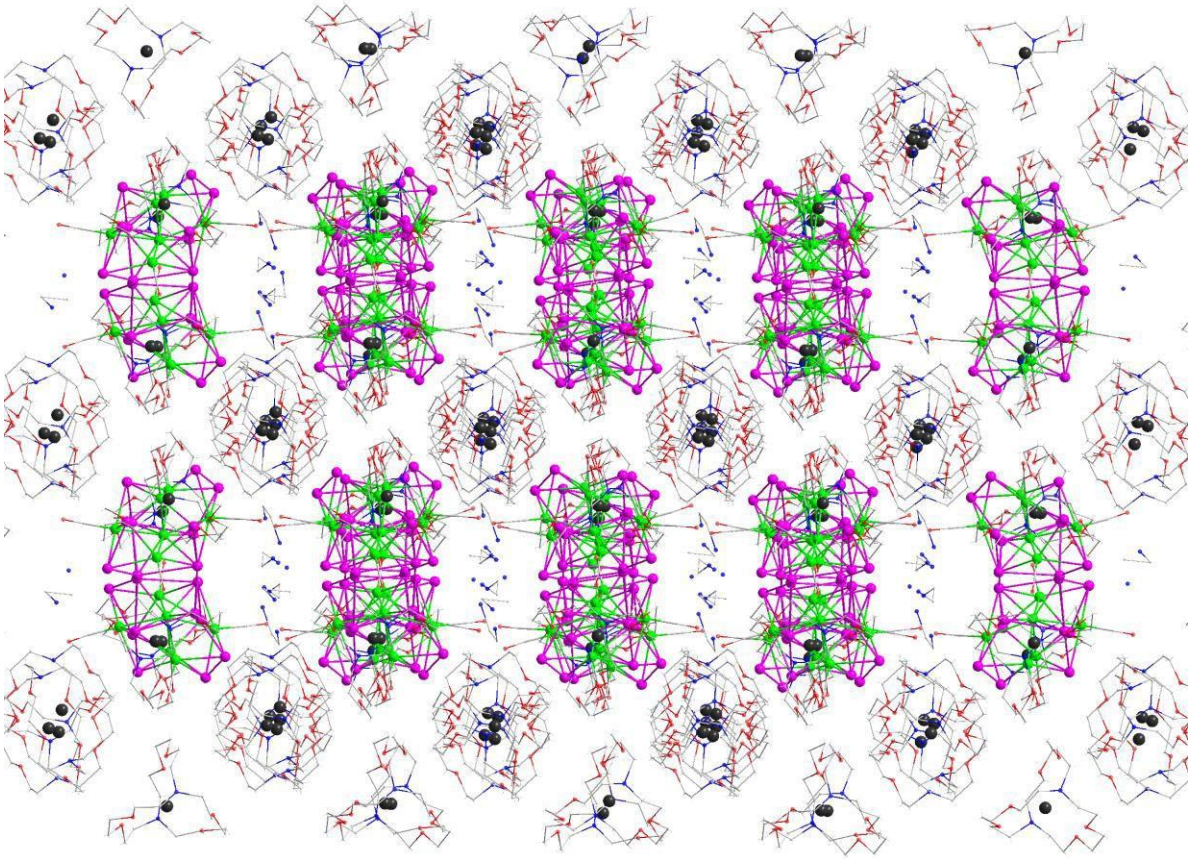

Figure S5. Crystal structures of [K(2,2,2-Crypt)]$_4$[**1**]·3*en*.

S6. Computational Methods and Details

All calculations on experimental structures of anions 1 and 1a was performed using Gaussian 16 program[2] at the pbe1pbe/def2tzvp level of theory.[3, 4] In these calculations, the solvent effects were taken into account by polarizable continuum model (PCM).[5] Figure 2 showed the orbital energy levels of the anions 1. We also performed the charge decomposition analysis (CDA)[6] using Multiwfn,[7] which is a multifunctional wave function analysis program using the files generated from the Gaussian calculations. Results of these analyses were summarized in Table S4. Figure S7 pointed out the occurrence of electron transfer from the polybismuthide anions to the Rh metal fragments. The NPA analyses[8] on clusters 1a were carried out by using Chemcraft and the results were presented in Table S6. To clarify the chemical bonding patterns of 1a and 1, we calculated the Mayer/Fuzzy bond orders[9, 10] (see Table S7-S8) and performed the Adaptive Natural Density Partitioning (see Figure S9 – S14) analyses[11] on the experimental structures by using Multiwfn. The ChemCraft 1.8 software was used for drawing molecular orbitals.

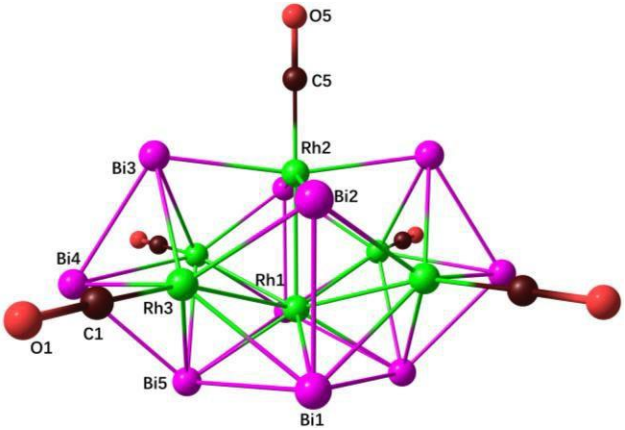

Figure S6. Optimised configuration of C_{2v}-**1a**(opt-**1a**).

Table S4. Results of the charge decomposition analysis (CDA) on the cluster ion opt-**1a.**

Orbital	Occupancy	Donation	Back donation	Charge polarization
HOMO-135	2.00	0.14204	0.00756	0.00601
HOMO-133	2.00	0.08865	0.02388	0.03701
HOMO-132	2.00	0.07452	0.02984	0.09476
HOMO-131	2.00	0.09932	0.02002	0.14604
HOMO-129	2.00	0.04852	0.01564	0.14440
HOMO-126	2.00	0.02401	0.00127	0.17071
HOMO-125	2.00	0.13685	0.01930	0.19020
HOMO-124	2.00	0.02151	0.00178	0.05818
HOMO-121	2.00	0.01282	0.00271	0.06585
HOMO-57	2.00	-0.00036	0.00163	-0.00230
HOMO-56	2.00	-0.00022	-0.00149	-0.00203
HOMO-50	2.00	-0.00038	-0.00177	-0.00209
HOMO-47	2.00	-0.00019	-0.00217	-0.00112
HOMO-10	2.00	0.0027	-0.00001	-0.00034
HOMO-9	2.00	0.0026	-0.00001	0.00036
HOMO-8	2.00	0.0028	-0.00001	0.00025
HOMO-7	2.00	0.0029	-0.00001	0.00020
HOMO-6	2.00	0.0016	-0.000003	0.00014
HOMO-5	2.00	0.0016	-0.000003	0.00009
HOMO-4	2.00	0.0035	-0.00001	0.00054
HOMO-3	2.00	0.0035	-0.00002	0.00055
HOMO-2	2.00	0.0044	-0.00002	0.00034
HOMO	2.00	0.0044	-0.00002	0.00036

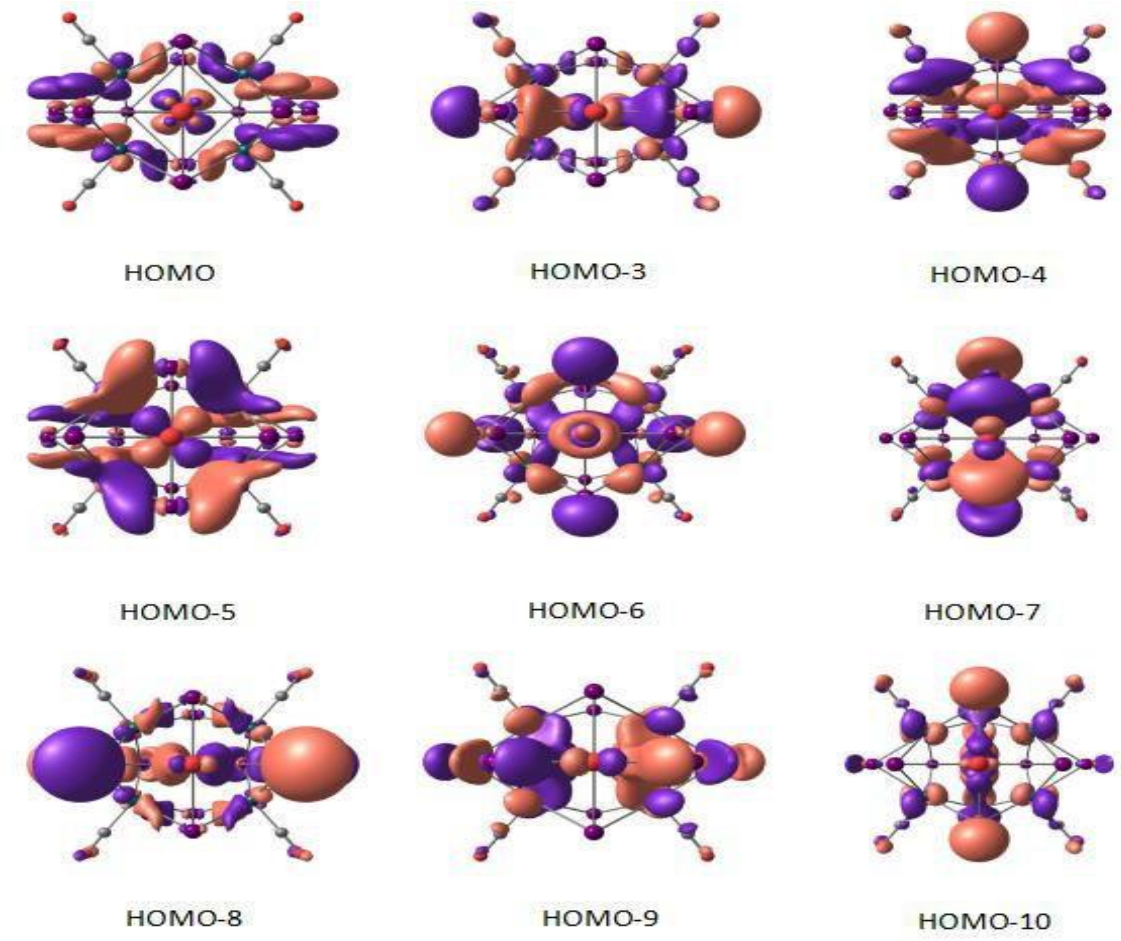

Figure S7. Representative occupied molecular orbitals of the anion opt-**1a**. All these orbitals contribute to the Bi-Rh bonds leading to the Bi to Rh charge transfer.

Table S5. Charge decomposition (CDA) analysis of opt-**1a**, $[Rh@Bi_9(RhCO)_5]^{3-}$ and $[Rh@Bi_{10}(RhCO)_6]^{3-}$.

	CDA between 1a and 1b(1a to 1b)	Bi to (RhCO)	Bi to Rh	(RhCO)
$[Rh@Bi_{10}(RhCO)_5]^{2-}$	0.0113	9.244	7.172	2.072
$[Rh@Bi_9(RhCO)_5]^{3-}$	No	9.5	7.640	1.86
$[Rh@Bi_{10}(RhCO)_6]^{3-}$	No	10.3	7.92	2.38

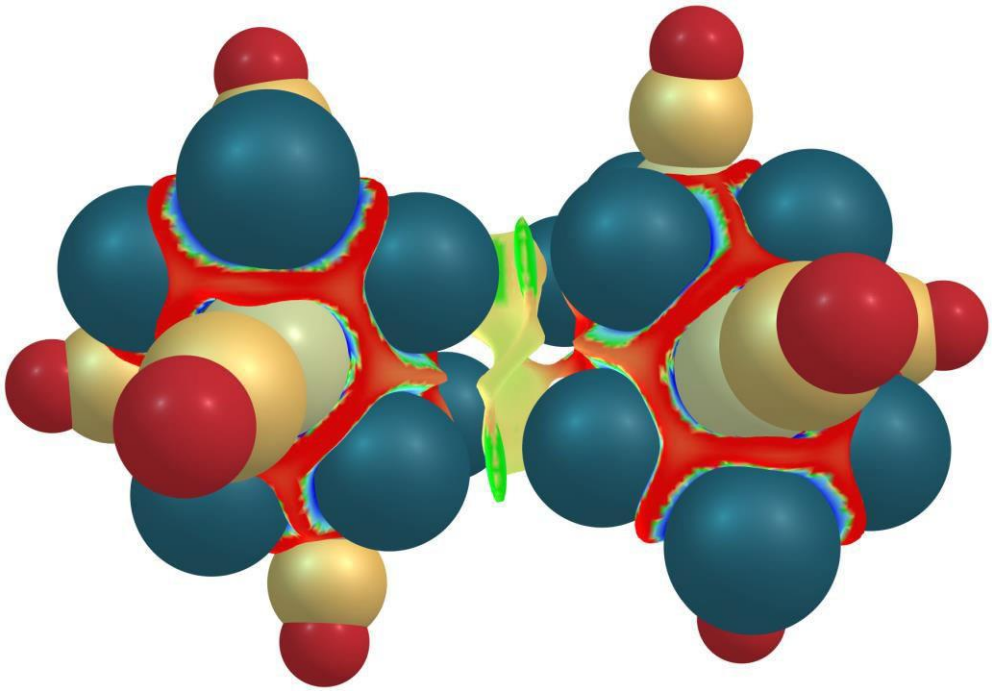

Figure S8. Stereo RDG diagram of **1**.

Table S6. Natural Population Analysis (NPA) of opt-**1a**.

1a	
Atom	Net charge
Bi1	0.711
Bi2	0.842
Bi3	0.701
Bi4	0.398
Bi5	0.562
Rh1	-1.169
Rh2	-1.483
Rh3	-1.622

Table S7. Distances, MBOs, and FBOs of the short Bi-Bi, Rh-Bi and Rh-Rh bonds in the heterometallic cluster ions opt-**1a**. The Bi and Rh atoms are defined in **Figures S4.**

	Distance (Å)	MBO	FBO
Bi1-Bi2	3.153(6)	0.60	0.67
Bi3-Bi4	3.007(4)	0.74	0.87
Bi4-Bi5	2.971(9)	0.82	0.92
Bi5-Bi1	3.480(3)	0.24	0.30
Bi5-Bi6	3.471(3)	0.24	0.30
Rh1-Rh2	2.7644(1)	0.14	0.58
Rh1-Rh3	2.8057(2)	0.14	0.50
Rh2-Bi3	2.7425(2)	0.61	0.86
Rh2-Bi2	2.7005(2)	0.57	0.85
Rh1-Bi1	2.7104(1)	0.50	0.85
Rh1-Bi5	2.6848(1)	0.60	0.91
Rh3-Bi1	2.8058(2)	0.55	0.78
Rh3-Bi2	2.7444(1)	0.66	0.87
Rh3-Bi3	2.7448(2)	0.56	0.78
Rh3-Bi4	2.8383(2)	0.50	0.83
Rh3-Bi5	2.9367(1)	0.41	0.65

Table S8. Average bond orders in opt-**1a** (**Figures S3**).

	Mayer average bond order	Fuzzy average bond order
Bi1-Bi2	0.55	0.58
Bi3-Bi4	0.69	0.80
Bi4-Bi5	0.82	0.9
Bi(1;5;10;6)-Bi(15;11;16;20)	0.08	0.24
Bi(2,3,7,8)-Rh_a	0.80	0.85
Bi(4,9)-Rh_m	0.53	0.81
Bi(1,5,6,10)-Rh_c	0.39	0.82
Bi(1;6)-Rh(3,6;4,5)	0.54	0.75
Bi(5;10)-Rh(3,4;5,6)	0.37	0.57
Bi(2;7)-Rh(3,6;4,5)	0.72	0.87
Bi(3;8)-Rh(3,4;5,6)	0.67	0.81

Rh_c = central Rh; Rh_a = apical Rh,Rh_m = middle Rh.

Table S9. Comparison of bond lengths of **1a** and opt-**1a.**

	1a-Distance (Å)	opt-**1a**-Distance (Å)
Bi1-Bi2	3.153(6)	3.07(4)
Bi3-Bi4	3.007(4)	2.97(0)
Bi4-Bi5	2.971(9)	2.97(0)
Bi5-Bi1	3.480(3)	3.51(6)
Rh1-Rh2	2.7644(1)	2.75(0)
Rh1-Rh3	2.8057(2)	2.83(8)
Rh2-Bi3	2.7425(2)	3.26(3)
Rh2-Bi2	2.7005(1)	2.72(5)
Rh1-Bi1	2.7104(1)	2.70(0)
Rh1-Bi5	2.6848(1)	2.68(2)
Rh3-Bi1	2.8058(2)	2.81(3)
Rh3-Bi2	2.7444(1)	2.77(2)
Rh3-Bi3	2.7448(2)	2.82(1)
Rh3-Bi4	2.8383(2)	2.82(0)
Rh3-Bi5	2.9367(1)	2.90(0)

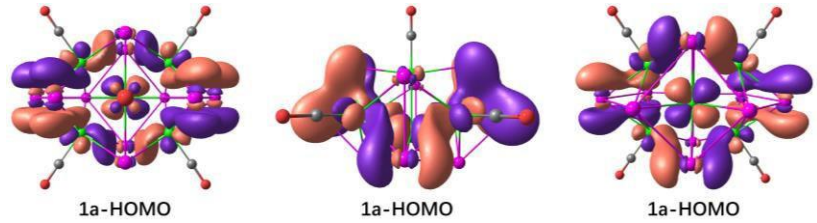

Figure S9. HOMO diagrams of different orientations for 1a.

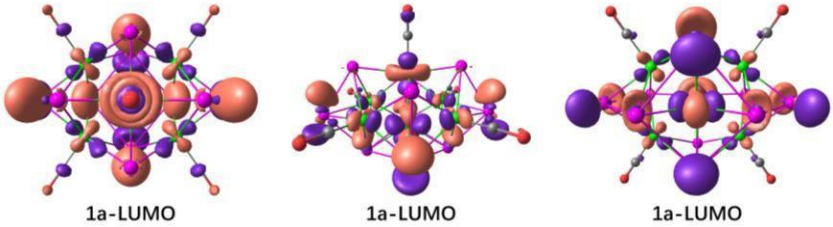

Figure S10. LUMO diagrams for different orientations of 1a.

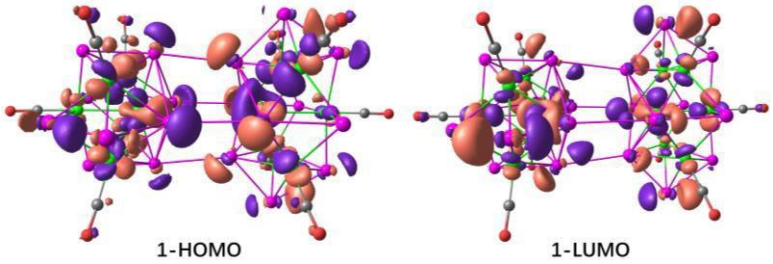

Figure S11. HOMO-LUMO diagram of 1.

Multicenter-2 electron (mc-2e) bonds with occupation number (ON)

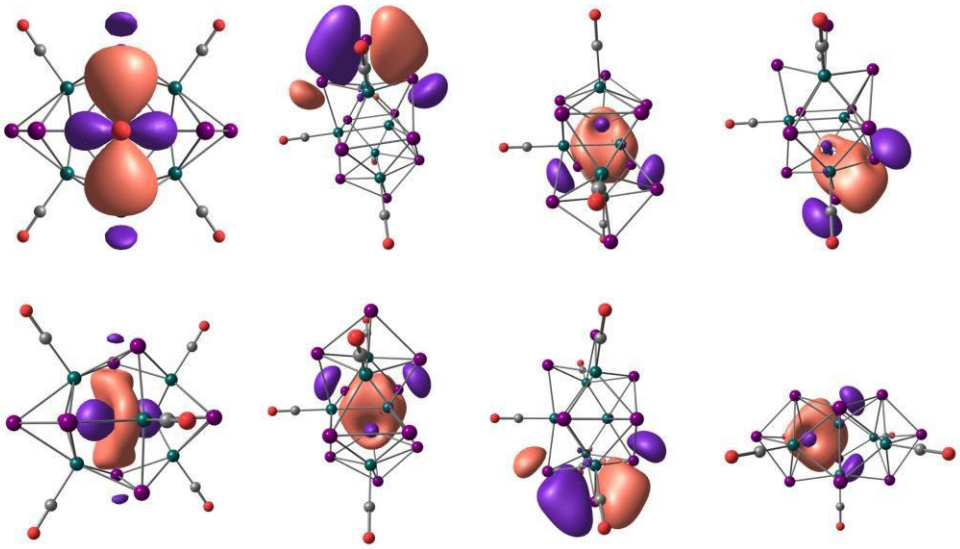

Figure S12. 3c-2e bonds, ON=1.73-1.95|e|.

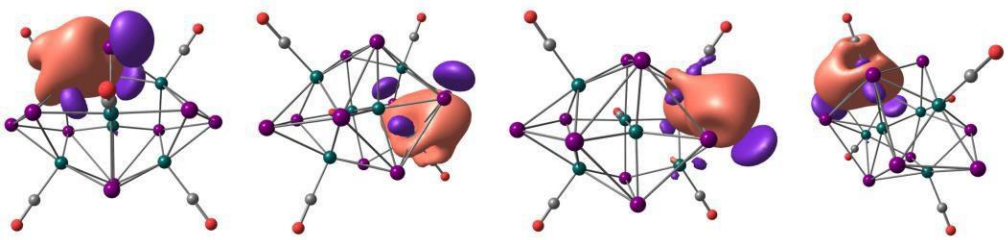

Figure S13. 4c-2e bonds, ON=1.82-1.87|e|.

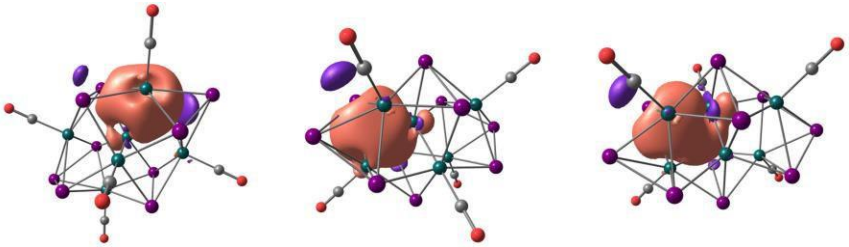

Figure S14. 4c-2e bonds, ON=1.72-1.78|e|.

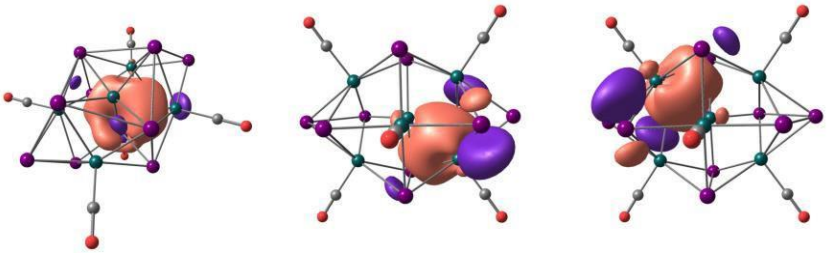

Figure S15. 5c-2e bonds, ON=1.72-1.80|e|.

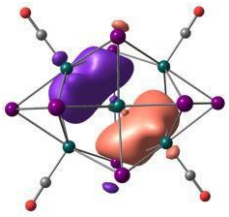

Figure S16. 7c-2e bonds, ON=1.76|e|.

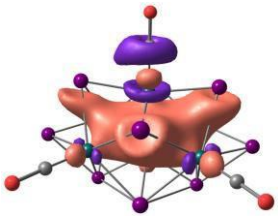

Figure S17. 9c-2e bonds, ON=1.73|e|.

S7. References

1. F. Gascoin and S. C. Sevov , "Synthesis and characterization of the "metallic salts" A_5Pn_4 (A = K, Rb, Cs and Pn = As, Sb, Bi) with isolated zigzag tetramers of Pn4(4-) and an extra delocalized electron.", *Inorg. Chem.*, 2001, **40**, 5177.
2. J. F. G. M, W. Trucks, H. B. Schlegel, G. E. Scuseria, M. A. Robb, J. R. Cheeseman, G. Scalmani, V. Barone, B. Mennucci, G. A. Petersson, Gaussian 09, Revision A. 1, *Gaussian*, 2009.
3. A. Schäfer, H. Horn and R. Ahlrichs, Theoretical study of the bond dissociation energies of methano, *J. Chem. Phys.*, 1992, **97**, 2571-2577.
4. (a) Bayat, Mehdi and N. Ahmadian , Bis-N-heterocyclic carbene in stabilized [bis-NHC(R) → EBr_2H_2] (E = Si to Pb) (R = H, F, Cl, Br, CH_3, CF_3) complexes: A theoretical study, *Polyhedron*, 2015, **96**, 95-101; (b) José Geraldo M. Castro Júnior and W. R. Rocha ,Theoretical investigation of $[Ru(bpy)_2(HAT)]^{2+}$ (HAT=1,4,5,8,9,12-hexaazatriphenylene; bpy=2,2′-bipyridine): Photophysics and reactions in excited state, *Spectrochim Acta A*, 2022, **270**, 120817.
5. S. Miertuš, E. Scrocco and J. Tomasi, Continuum solvation models in chemical physics: from theory to applications, *Chem. Phys.*, 1981, **55**, 117-129.
6. (a) H. Jacobsen, A. Correa, A. Poater, C. Costabile and L. Cavallo, Understanding the M(NHC) (NHC=N-heterocyclic carbene) bond, *Coordin Chem Rev*, 2009, **253**, 687-703; (b) S. Dapprich and G. Frenking, Investigation of Donor-Acceptor Interactions: A Charge Decomposition Analysis Using Fragment Molecular Orbitals, *J. Phys. Chem. C*, 1995, **99**, 9352-9362.
7. T. Lu and F. Chen, Multiwfn: A multifunctional wavefunction analyzer, *J Comput Chem*, 2012, **33**, 580-592.
8 G. Bruhn, E. R. Davidson, I. Mayer and A. E. Clark, Löwdin population analysis with and without rotational invariance, *Int J Quantum Chem*, 2006, **106**, 2065-2072.
9. (a) A. J. Bridgeman, G. Cavigliasso, L. R. Ireland, et al, The Mayer bond order as a tool in inorganic chemistry, *J. Am. Chem. Soc*, 2001, 2095-2108; (b) T. Lu and F. Chen, Bond order analysis based on the laplacian of electron density in fuzzy overlap space, *J. Phys. Chem. A*, 2013, **117**, 3100-3108.
10. D. Y. Zubarev and A. I. Boldyrev, Developing paradigms of chemical bonding: adaptive natural density partitioning, *Phys. Chem. Chem. Phys.*, 2008, **10**, 5207-5217.